Computational prediction of samarium hydride at megabar pressure

[1]Zelong Zhao, [2]Siyu Chen, [2,3]Bartomeu Monserrat, [1*]Evgeny Plekhanov,* and [1*]Cedric Weber†
[1] *Theory and Simulation of Condensed Matter(TSCM), King's College London, The Strand,London WC2R 2LS,UK*
[2] *TCM Group, Cavendish Laboratory, University of Cambridge, J. J. Thomson Avenue, Cambridge CB3 0HE, United Kingdom and*
[3] *Department of Materials Science and Metallurgy, University of Cambridge, 27 Charles Babbage Road, Cambridge CB3 0FS, United Kingdom*

Samarium hydrides, a group of physically viable lanthanide polyhydrides, have yet to be experimentally realized at high pressures. In this work, we combine the first-principles methods of density functional theory (DFT) with dynamical mean-field theory (DMFT) to explore the many-body correlations of samarium. We explore various stoichiometries of samarium hydrides via random structure searches across a range of pressures and report the SmH_2 with a layered hexagonal structure in the $P6/mmm$ space group to a theoretically stable phase at a high pressure of approximately 200 GPa.

arXiv:2208.01577v1 [cond-mat.str-el] 2 Aug 2022

I. INTRODUCTION

Much recent research on superconductivity has focused on lanthanum hydrides [1] due to their high superconducting critical temperature (T_c) at high pressure. Since then, many lanthanide hydrides [2] have been studied either experimentally [1] or computationally [3, 4]. Among lanthanide hydrides, samarium hydride has not been well studied. Experimentally, samarium hydride has only been studied at ambient pressure [5]; computationally, theoretical predictions of samarium hydride under high pressure is still lacking.

Superconductivity was fist observed early in the 20th century and has since motivated a long-standing quest toward achieving high critical temperatures. In particular, the discovery of high-critical-temperature materials, such as the copper oxides, in the 1980s has generated a tremendous revival of interest in identifying room temperature superconductors. Two mechanisms have been suggested to account for superconductivity: i) the early proposal of Bardeen-Cooper-Schrieffer [6] in which electrons pair via phonon-mediated interactions, which accounts for type-I superconductors, ii) and spin fluctuations which accounts for the type-II high-T_c materials.

Early on, Ashcroft [7, 8] suggested that type-I superconductors could achieve a large T_c provided that the phonon frequency was large enough, typically in light element systems, such as hydrides, at high pressures. Metallic hydrogen [7, 8] is predicted to have a T_c higher than room temperature at extreme pressure [9]. However, alternatives, typically combining "metallic hydrogen" with other elements, have been suggested to enhance stability at experimentally achievable pressures. The aim of these method is to reduce the pressure of the stable phase of the hydrogen-rich system but maintain the high frequency and electron-phonon coupling strength of metallic hydrogen. The latter obviously comes with a large scope of possible candidates, with a range of chemical compositions but also different stoichiometries and possible symmetry group or lattice structures. Computational studies [10, 11] have provided possible candidates of high-T_c superconductors (HTSCs). More importantly, a previous study showed that the superconductivity of lanthanide hydrides is phonon-mediated [1]. This class of material attracts the attention of computational physicists to apply existing computational methods to calculate their superconductivity properties [12].

Identifying stable phase depends on crystal structure prediction methods[13–15], in particular, first-principles calculations are typically being carried out via the standard density functional theory (DFT) across a wide range of structures and compositions. As this is a laborious process, recent advances have allowed for searching across the vast landscape of possible structures. The main DFT schemes used in majority of random structure search is seeking relaxed phase. Nonetheless, non-local treatment of standard DFT method does not meet satisfactory result for transition metal and rare earth element [16]. One way to counter this effect is to include further treatment of those correlated electron with local or semi-local level.

Theoretical predictions of samarium hydrides at high pressure are not attainable before experimentally observing the high pressure phase transition of samarium [17]. Guided by this experiment, we make use of high pressure conditions [17, 18] to explore the possible stoichiometries of samarium hydride. In this work, we use ab initio random structure search code (AIRSS)[15, 19] to study the stability of this compound. The accuracy of the enthalpy determined for each generated cell depends on quantum solver; here, DFT+U [20] is implemented to treat geometry optimisation calculations via plane wave code (CASTEP) [21]. AIRSS finds a number of possible candidates of Sm_yH_x, x (1∼18) and y (1∼2), under external pressures ranging from 1 to 400 GPa (Fig. S1). SmH_2 $P6/mmm$ is identified as the most stable phase. In particular, the electronic properties and superconductivity of the stable phase are studied under 200 GPa. The electronic structure of this compound is studied with the state-of-the-art DFT+DMFT method. The rest of this

* evgeny.plekhanov@kcl.ac.uk
† cedric.weber@kcl.ac.uk

paper is organised as follows: computational details of the method, followed by a discussion of the results.

II. METHOD

A. Theory

Within the Density Functional Theory (DFT) [22, 23] the many-body Schrödinger equations are solved by mapping the problem onto an auxiliary one-body problem with the same electronic density. This auxiliary system is usually called the Kohn-Sham (KS) system, and the electrons therein experience an effective potential $V_{\text{eff}}(\mathbf{r})$:

$$\left[-\frac{\hbar^2}{2m}\nabla^2 + V_{\text{eff}}(\mathbf{r})\right]\varphi_i(\mathbf{r}) = \varepsilon_i\varphi_i(\mathbf{r})$$
$$V_{\text{eff}}(\mathbf{r}) = V(\mathbf{r}) + \int \frac{n(\mathbf{r}')}{|\mathbf{r}-\mathbf{r}'|}\mathrm{d}^3\mathbf{r}' + V_{\text{XC}}[n(\mathbf{r})] \quad (1)$$

$\varphi_i(\mathbf{r})$ is the i-th KS orbital, and the electronic density $n(\mathbf{r})$ is derived from the densities of the KS orbitals occupied up to the Fermi level. The accuracy of DFT depends on the choice of exchange correlation (XC) functional. Various levels of approximation include Local Density Approximation (LDA), Generalized Gradient Approximations (GGA), etc. In this work, we adopt Perdew-Burke-Ernzerhof (PBE) XC functional [24].

However, the amount of correlations, contained in the DFT XC functional, is not sufficient to treat the strong Coulomb repulsion in partially filled d and f orbitals. Within the standard DFT, these strongly correlated orbitals appear to be excessively delocalized. This lack of localization can be to some extent corrected with the DFT+U scheme, where the DFT energy functional is supplied with an additional term, proportional to a parameter, called Hubbard U, which penalizes the configurations with doubly occupied orbitals [25].

A higher level treatment of the strong Coulomb repulsion is provided within DFT + Dynamical Mean Field Theory (DFT+DMFT) approach [26–28], where the temporal correlations are taken into account exactly, while the treatment of the spatial ones becomes exact in the limit of infinite coordination of the correlated orbital. Within DFT+DMFT, a problem of a correlated orbital (usually d or f, or a subset of the formers), connected to a chemical environment, is mapped onto an auxiliary problem of an Anderson impurity connected to a bath of "uncorrelated" orbitals. The latter problem is then solved either numerically (quantum Monte Carlo, exact diagonalization etc.) or analytically by using some approximation (Hubbard-I, auxiliary bosons etc). The results of such an impurity problem are then mapped back onto the original correlated lattice problem. The details of the DFT+DMFT implementation used in the present work can be found in the Refs. 28 and 29.

Once the structure is obtained, we use DFT+DMFT to correct the electronic properties under the assumption that the structure is well estimated by DFT+U. The efficiency of the random structure search is crucial for searching low enthalpy compounds. Several tactics can be used, including the adjustment of the volume and low-resolution energy surface during the initial scan, followed by high-precision calculations. To obtain the convex hull of this material, we used a simple chemical reaction method to calculate the enthalpy of formation:

$$\mathrm{Sm}_y\mathrm{H}_x = x\,\mathrm{H} + y\,\mathrm{Sm} \quad (2)$$

Phases of samarium [17] and hydrogen [18] are stable at the pressure considered in the present work. For example, under 200 GPa, hydrogen is in the $C2/c$ phase and samarium is in the $oF8$ phase. The formation enthalpies found by this method are likely to be overestimated due to the oversimplified reaction pathway. Moreover, these formation enthalpies are larger in magnitude than any other synthetic pathway, since the enthalpies of the possible compounds forming SmH_x would be much lower. Furthermore, neglecting higher enthalpy compound among same space group might miss other possible candidates especially for low symmetry space group compound such as P-1, $C2/m$, etc. (see Fig. S2).

B. Computational details

In the present work, we have performed the ab-initio calculations by using CASTEP and Quantum Espresso codes. The GGA in the Perdew-Burke-Ernzerhof (PBE) variant and ultra soft pseudo potential (USPP) for $\mathrm{Sm}([\mathrm{Xe}]4\mathrm{f}^6 6\mathrm{s}^2)$ $\mathrm{H}(1\mathrm{s}^1)$ were used for all kind of DFT calculations.

The random structure search for a stable phase of $\mathrm{Sm}_y\mathrm{H}_x$ stoichiometry was performed by using AIRSS [15] and CASTEP [21]. DFT+U calculations were carried out at U = 3eV and 6eV, and the spin polarized geometry optimization was done starting from the results of the random structure search. Two-steps approach was adopted in order to enhance the random structure search: step 1) the AIRSS exploration of different stoichiometries with a coarse Monkhorst-Pack (MP) **k**-point grid ($2\pi\times$ 0.03 Å^{-1}), kinetic energy cut-off E_{cut} = 500eV, force tolerance 0.05 eV/Å, U = 3eV; step 2) on a smaller subset of structures having the lowest enthalpy within each symmetry group, the calculations with finer parameter set were run: denser MP **k**-point grid ($2\pi\times$ 0.01 Å^{-1}), E_{cut} = 600 eV, U = 3 eV and the force tolerance 0.001 eV/Å. We note that the parameter set used in step 2) ensures that the overall energy precision is within 1 meV/per atom (see Fig. S3).

We have performed the DFT+DMFT calculations as implemented within CASTEP [21, 28, 29] with the same DFT parameters as the ones used in the "step 2", except

for the Hubbard U, which was taken to be $U = 6$ eV and an additional Hund's coupling J with $J = 0.855$ eV.

The phonon dispersions were calculated in the harmonic approximation using finite differences [30] combined with the non-diagonal supercells [31] technique. The **q** points grids for Brillouin zone sampling was $6 \times 6 \times 6$.

Electron-phonon coupling properties are calculated via a density functional perturbation theory (DFPT) algorithm. The **q** point grids used to sample in the Brillouin zone are coarse $6 \times 6 \times 6$. The DFT settings involved in the DFPT calculation are identical to those used in "step 2". Furthermore, the superconductivity temperature is found via Allen and Dynes [32] revised McMillan [33] equation implemented in Quantum Espresso [12].

III. RESULT AND DISCUSSION

A. Structure Search

The random structure search was run a thousand times in order to identify a stable phase. As a result, SmH_2 appears to be the most stable phase. In particular, 52 structures were generated for Sm_2H_4 and SmH_2 at 200 GPa (figure: S1). The lowest enthalpy was found for $SmH_2(P6/mmm,F\text{-}43m,Cm)$ $Sm_2H_4(P6/mmm,I4_1/amd,Cmmm)$. The quality of our random structure search is confirmed by the fact that we have recovered several samples of ground state polycrystals, such as $P6/mmm$. In order to optimize the usage of computational resources, we have adopted the two-step procedure outlined above. The structures we have found tend to possess a high symmetry at high pressure.

The results of the random structure search can be illustrated by the convex hull structure (Fig. 1). Each point is a structure with a certain pressure and stoichiometry found by a random structure search. In this structure, the x-axis is the ratio of hydrogen atoms relative to the total number of atoms in their cell, in one formula unit (f.u.). The left side, x = 0, is hence the samarium bulk, and the right side, x = 1, is the hydrogen bulk. The dashed line indicates instability and the solid line indicates the stable phase. This method identifies the stable and unstable phases by comparing the linear change in enthalpy with the change in components.

We find that higher precision (Fig. S2) does not change the overall sequential order of the low-enthalpy phases; i.e., $P6/mmm$ remains the most stable phase in this case. Several other phases also evolve to $P6/mmm$. In terms of enthalpy, at 200 GPa, one of our most stable phases (SmH_2 $P6/mmm$, Fig. 1 (b)) recovers a known structure, the "ScH2" phase obtained in [4]. Interestingly, the predicted possible structure of SmHx is highly symmetric and common to other high-pressure lanthanide hydride phases. We point out that the enthalpy of elemental hydrogen at very high pressures is entered in the calculation of the formation energy. However, this remains an open

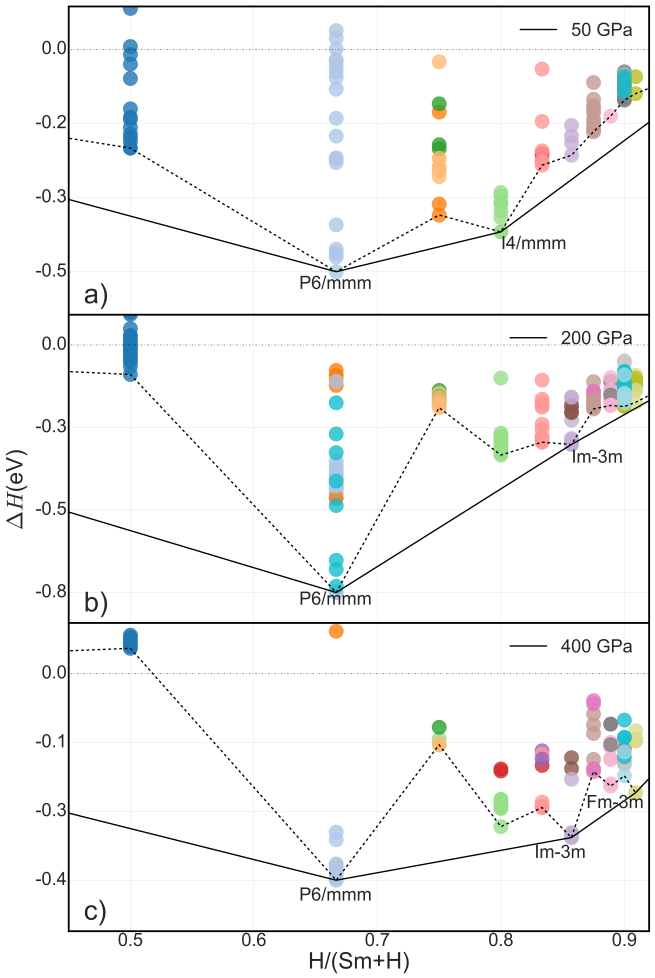


FIG. 1. Maxwell Convex hull analysis of 50,200,400 GPa. Solid line indicate stable phase, dashed line indicate unstable phase and dashed dot line is plotted at y equal to zero, above this line means compound has even higher enthalpy than hydrogen C2/c [18] and samarium of8. [17]

question in itself, since metallic hydrogen has been predicted in our pressure regime [8]. In this work, we use the theoretical estimates of solid hydrogen [18]. Furthermore, our results remain stable in terms of a reasonable variation of the estimated H enthalpy, and in particular the order of the obtained phases remains the same (figure 1) as well.

Between 50 GPa and 400 GPa, SmH_2 (Fig. 2) is the most stable phase. It exhibits a layered structure similar to MgB_2. The meta-stable phase between 50 and 140 GPa is SmH_4. The meta-stable phase then moves towards more hydrogen-rich compounds as expected. The structure obtained with the $Immm4$ symmetry group of SmH_4 is the most stable phase in [4]. However, this is not the case in our results, as we have identified competing phases. In particular, we found (Fig. 2 b) the predicted ground state to be $P6/mmm$, while $Immm4$ is the metastable phase until 80 GPa.

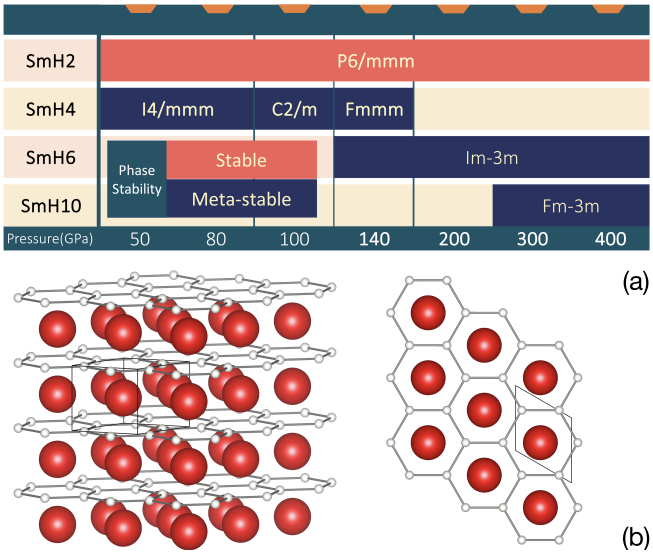


FIG. 2. (a) stable phase and meta-stable phase for Sm. Pink stands for the stable phase, and blue represents the meta-stable phase. P6/mmm is always the stable phase. Meta-stable phase tends to have more hydrogen as pressure increases. (b) P6/mmm for SmH_2

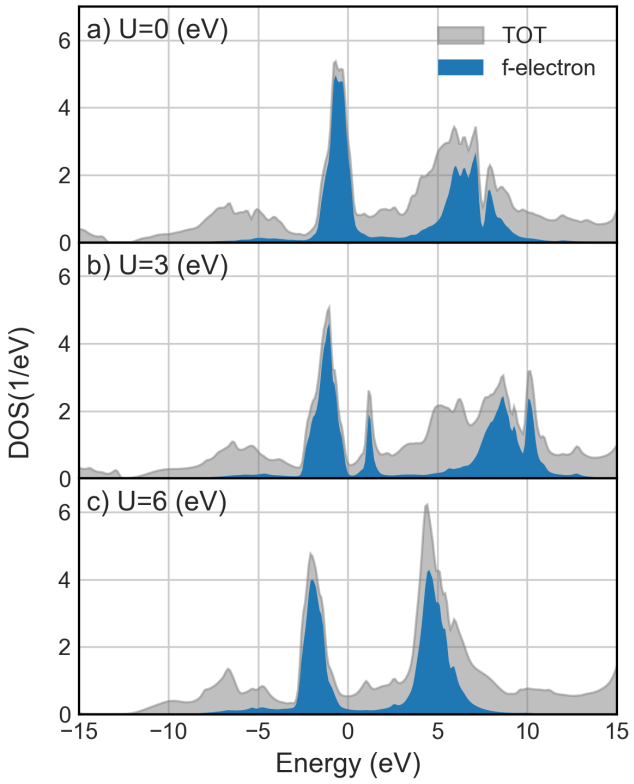


FIG. 3. DOS of $P6/mmm$ predicted by DFT and DFT+U with kinetic energy cutoff of 600 eV, $\mathbf{k}$ mesh $2\pi \times 0.01$, PBE and USPP. a) DFT calculation. U=0 eV indicates DFT calculation. b) and c) DFT+U calculations with Hubbard U equal to 3 and 6 eV.

B. Electronic properties of $P6/mmm$

To investigate the electronic properties of SmH_2 of $P6/mmm$ phase, we calculated the corresponding partial density of states (PDOS) in (Fig. 3). Only samarium contributes f-electrons, and TOT indicates the total DOS of SmH_2. The PBE exchange functional splits the DOS of the 4f electrons and causes steep negative slop at the Fermi level. The Hubbard U term in the DFT+U method includes the Mott transition via splitting the DOS of correlated orbitals and pushing the pseudo-particle peak away from the Fermi level. Both DFT+U with U (3 eV and 6 eV) predict the samarium 4f electrons peak away from the Fermi level.

Phonon dispersion of $P6/mmm$ at 200 GPa of either DFT or DFT+U has no soft modes, which indicates that the predicted phase is dynamically stable. Phonons of samarium hydrides have similar parttens as other lanthanides hydrides. The gap between optical and acoustical branches is distinct as great difference of mass between lanthanides elements and hydrogen. In contrast, the Hubbard U term has a negligible effect on phonon dispersion. Under different values of Hubbard U, the equilibrium volume of P6/mmm varies from 15.72(Å) to 16.45(Å) for U equals to 0 eV and 6 eV respectively. The effect of Hubbard U term on the force was nearly eliminated out by changing in volume.

To capture the correlation effects of f-electrons, we carried out DFT+DMFT calculations for SmH_2 $P6/mmm$ at 200 GPa. We reached different degrees of convergence (Fig. 5). 1-shot indicates the convergence of the chemical potential μ, and charge self-consistency (CSC) refers to the fact that the charge number is consistent with the charge density. In this case, the chemical potentials of DFT+U (Fig. 3) and DFT+U (Fig. 3 (b)) and DFT+DMFT (Fig. 5) show similar charge densities. (a)) show similar density of states at the Fermi level. Unlike DFT+U, the Hund's coupling J, Hubbard U also plays a role (see Figs. S4, S5). DMFT corrections on the other hand produce spectral function. A full-fledged charge consistency calculation increased DOS of Samarium 4f and H 1s electrons.

We further performed density perturbation theory (DFPT) calculations to estimate the electron-phonon coupling (EPC) and calculated the superconducting temperature (T_c) via the Allen and Dynes [32] revised McMillan [33] equation:

$$T_c = \frac{\omega_{\log}}{1.2} \exp\left[\frac{-1.04(1+\lambda)}{\lambda(1-0.62\mu^*)-\mu^*}\right] \quad (3)$$

Here, μ^* is Coulomb potential with typical value between 0.1 to 0.15. λ is electron-phonon coupling strength. $\omega_{\log}$ is logarithmic average frequency. They are evaluated via integral of Eliashberg dispersion function:

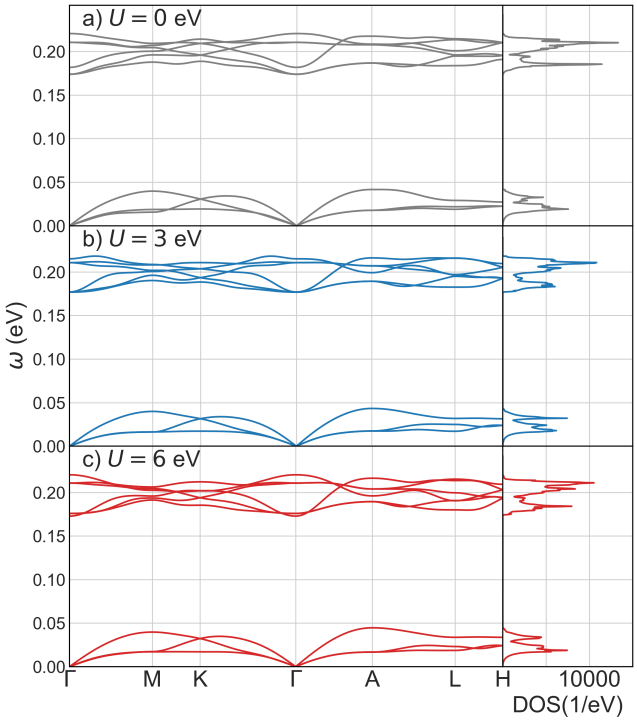


FIG. 4. The left side panel shows the P6/mmm phonon dispersion and the right side panel shows the phonon DOS. Both are calculated with a coarse q-point grid size of 6×6×6. Electronic method is DFT+U with U as indicated.

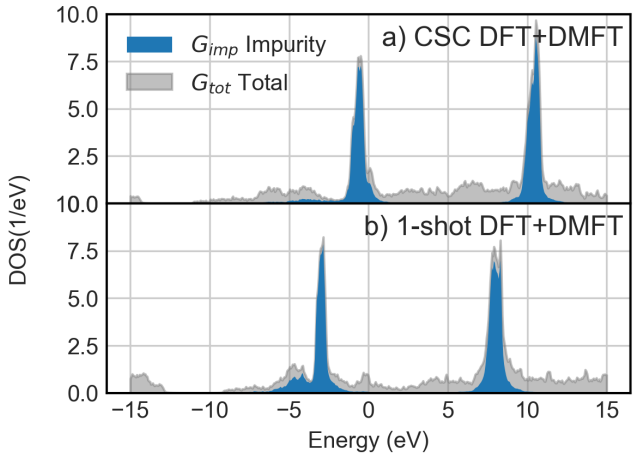


FIG. 5. DFT+DMFT density of state for P6/mmm at 200 GPa. Hubbard U, 6eV. Hund's coupling J=0.85eV. DC=3.1

$$\lambda = 2\int_0^\infty \frac{\alpha^2 F(\omega)}{\omega} d\omega$$
$$\omega_{\log} = \exp\left[\frac{2}{\lambda}\int \frac{d\omega}{\omega}\alpha^2 F(\omega)\log\omega\right] \quad (4)$$

λ of SmH_2 $P6/mmm$ is relatively low 0.28 and thus

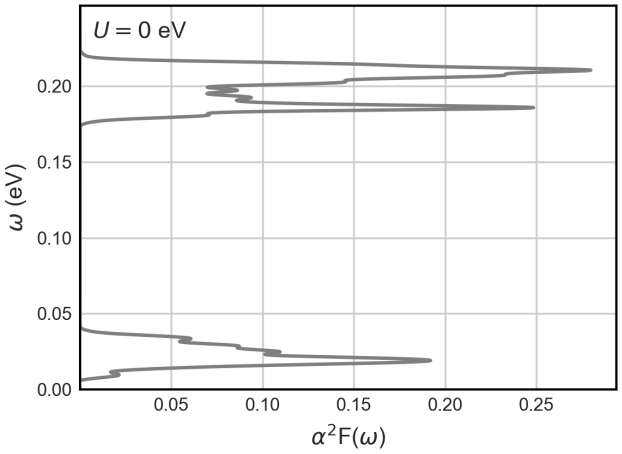


FIG. 6. Eliashberg equation of SmH_2 $P6/mmm$. **q** points grid is 6 × 6 × 6. Elements of electronic coupling matrix is calculated via DFPT.

T_c is less than 1 k for $\mu*$ between 0.1 and 0.15. This result is consistent with the previous publications [4, 34] in terms of decreasing T_c of lanthanide series hydrides with decreasing lanthanides (higher T_c for La/Y hydrides higher, while intermediate series of lanthanides, such as Sm, have lower T_c). The reason for the low T_c for samarium hydride could be caused by i) low hydrogen DOS at Fermi level, ii) week electron-phonon coupling strength.

In conclusion, we used random structure searches via the AIRSS method [15, 18, 19] for the family of the lanthanide hydrides. We focused on a material where the structure remains unknown experimentally at high pressures for different stoichiometry. We especially studied the 200 GPa. $P6/mmm$ is predicted to be the stable phase. Meta-stable phase are found for SmH_y for y equal to 4,6, and 10. As expected, this indicated that higher pressure samarium hydrides compounds could be hydrogen-rich. We then systematically studied the electronic structure and lattice stability. This work opens new avenues for studying hydrides at high pressure. As shown in this work, new highly symmetric phases of correlated matter can emerge, leading to a breadth of properties interesting for possible applications, such as superconductivity. The method used in this work is quite general and can be extended to other systems of interest.

ACKNOWLEDGEMENTS

CW and EP are supported by the grant [EP/R02992X/1] from the UK Engineering and Physical Sciences Research Council (EPSRC). This work was performed using resources provided by the ARCHER UK National Supercomputing Service and the Cambridge Service for Data Driven Discovery (CSD3) operated by the University of Cambridge Research Computing

Service (www.csd3.cam.ac.uk), provided by Dell EMC and Intel using Tier-2 funding from the Engineering and Physical Sciences Research Council (capital grant EP/P020259/1), and DiRAC funding from the Science and Technology Facilities Council (www.dirac.ac.uk).

S.C. acknowledges financial support from the Cambridge Trust and from the Winton Programme for the Physics of Sustainability.

B.M. acknowledges support from a UKRI Future Leaders Fellowship (Grant No. MR/V023926/1), from the Gianna Angelopoulos Programme for Science, Technology, and Innovation, and from the Winton Programme for the Physics of Sustainability.

[1] M. Somayazulu, M. Ahart, A. K. Mishra, Z. M. Geballe, M. Baldini, Y. Meng, V. V. Struzhkin, and R. J. Hemley, Physical Review Letters **122**, 027001 (2019).
[2] Y. Fukai, *The metal-hydrogen system: basic bulk properties*, Vol. 21 (Springer Science & Business Media, 2006).
[3] E. Plekhanov, Z. Zhao, F. Macheda, Y. Wei, N. Bonini, and C. Weber, Physical Review Research **4**, 013248 (2022).
[4] F. Peng, Y. Sun, C. J. Pickard, R. J. Needs, Q. Wu, and Y. Ma, Physical review letters **119**, 107001 (2017).
[5] J. Daou, P. Vajda, and J. Burger, Solid state communications **71**, 1145 (1989).
[6] J. Bardeen, L. N. Cooper, and J. R. Schrieffer, Physical review **108**, 1175 (1957).
[7] N. W. Ashcroft, Physical Review Letters **21**, 1748 (1968).
[8] N. Ashcroft, Physical Review Letters **92**, 187002 (2004).
[9] J. M. McMahon and D. M. Ceperley, Physical Review B **84**, 144515 (2011).
[10] D. C. Lonie, J. Hooper, B. Altintas, and E. Zurek, Physical Review B **87**, 054107 (2013).
[11] Y. Li, J. Hao, H. Liu, Y. Li, and Y. Ma, The Journal of chemical physics **140**, 174712 (2014).
[12] P. Giannozzi, S. Baroni, N. Bonini, M. Calandra, R. Car, C. Cavazzoni, D. Ceresoli, G. L. Chiarotti, M. Cococcioni, I. Dabo, *et al.*, Journal of physics: Condensed matter **21**, 395502 (2009).
[13] C. W. Glass, A. R. Oganov, and N. Hansen, Computer physics communications **175**, 713 (2006).
[14] Y. Wang, J. Lv, L. Zhu, and Y. Ma, Computer Physics Communications **183**, 2063 (2012).
[15] C. J. Pickard and R. Needs, Journal of Physics: Condensed Matter **23**, 053201 (2011).
[16] M. Imada, A. Fujimori, and Y. Tokura, Reviews of modern physics **70**, 1039 (1998).
[17] S. Finnegan, E. Pace, C. Storm, M. McMahon, S. MacLeod, H.-P. Liermann, and K. Glazyrin, Physical Review B **101**, 174109 (2020).
[18] C. J. Pickard and R. J. Needs, Nature Physics **3**, 473 (2007).
[19] C. J. Pickard and R. Needs, Physical Review Letters **97**, 045504 (2006).
[20] M. Cococcioni, Correlated Electrons: From Models to Materials Modeling and Simulation **2** (2012).
[21] S. J. Clark, M. D. Segall, C. J. Pickard, P. J. Hasnip, M. I. Probert, K. Refson, and M. C. Payne, Zeitschrift für kristallographie-crystalline materials **220**, 567 (2005).
[22] W. Kohn and L. J. Sham, Physical review **140**, A1133 (1965).
[23] P. Hohenberg and W. Kohn, Physical review **136**, B864 (1964).
[24] J. P. Perdew, K. Burke, and M. Ernzerhof, Physical review letters **77**, 3865 (1996).
[25] B. Himmetoglu, A. Floris, S. De Gironcoli, and M. Cococcioni, International Journal of Quantum Chemistry **114**, 14 (2014).
[26] A. Georges, G. Kotliar, W. Krauth, and M. J. Rozenberg, Reviews of Modern Physics **68**, 13 (1996).
[27] G. Kotliar, S. Y. Savrasov, K. Haule, V. S. Oudovenko, O. Parcollet, and C. Marianetti, Reviews of Modern Physics **78**, 865 (2006).
[28] E. Plekhanov, P. Hasnip, V. Sacksteder, M. Probert, S. J. Clark, K. Refson, and C. Weber, Physical Review B **98**, 075129 (2018).
[29] E. Plekhanov, N. Bonini, and C. Weber, Phys. Rev. B **104**, 235131 (2021).
[30] K. Parlinski, Z. Q. Li, and Y. Kawazoe, Phys. Rev. Lett. **78**, 4063 (1997).
[31] J. H. Lloyd-Williams and B. Monserrat, Phys. Rev. B **92**, 184301 (2015).
[32] P. B. Allen and R. Dynes, Physical Review B **12**, 905 (1975).
[33] W. McMillan, Physical Review **167**, 331 (1968).
[34] D. V. Semenok, I. A. Kruglov, I. A. Savkin, A. G. Kvashnin, and A. R. Oganov, Current Opinion in Solid State and Materials Science **24**, 100808 (2020).

Supplemental Materials: Computational prediction of Samarium Hayride at Magebar pressure

I. RANDOM STRUCTURE SEARCH

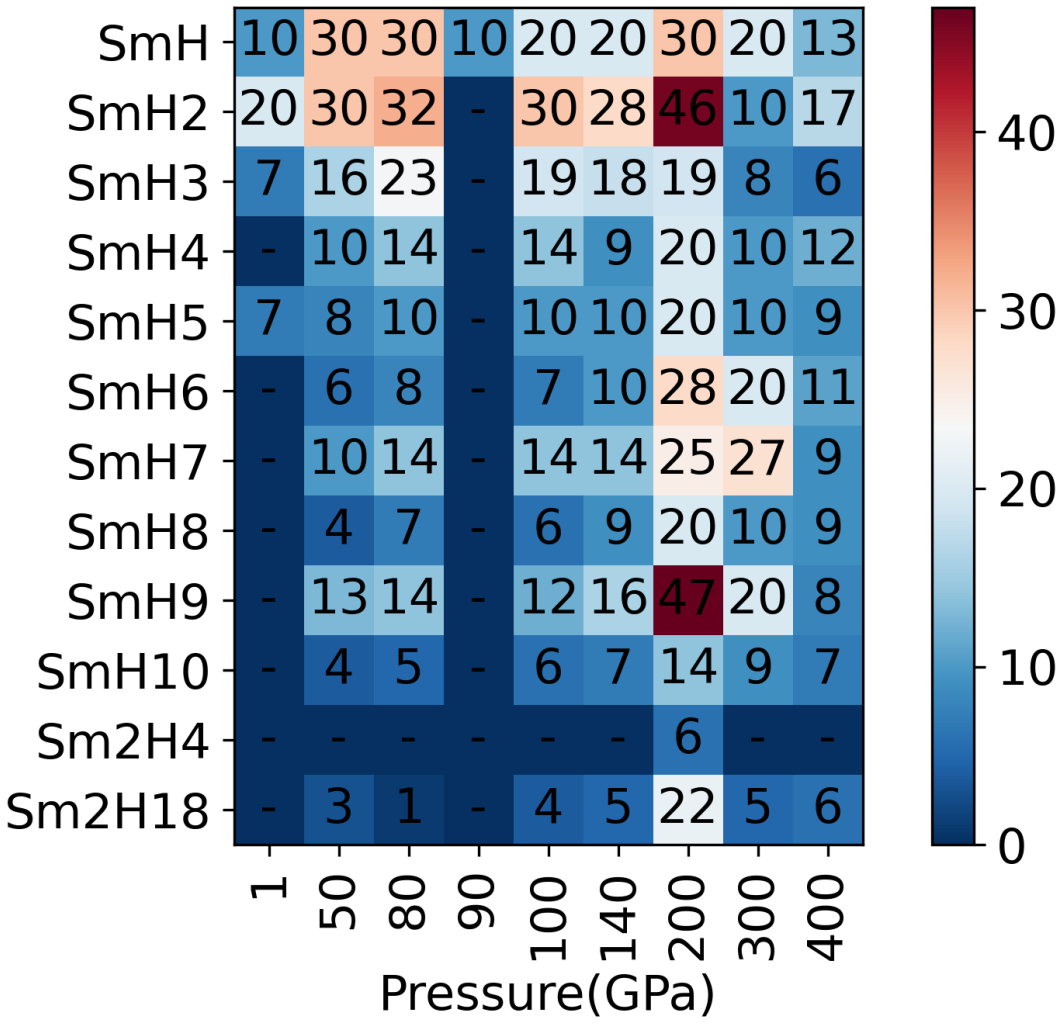


FIG. S1. Size of the phase database. Y-axis is stoichiometry of Samarium and hydrogen. X-axis is pressure we performed random structure search. Phase we searched "-" represents we did not search for this pressure and stoichiometry. The number indicated in each of the cell is the total number of distinct structure identified by AIRSS at each pressure for each stoichiometry. Colour bar blue for less search performed for this combination and red represents for more intense search.

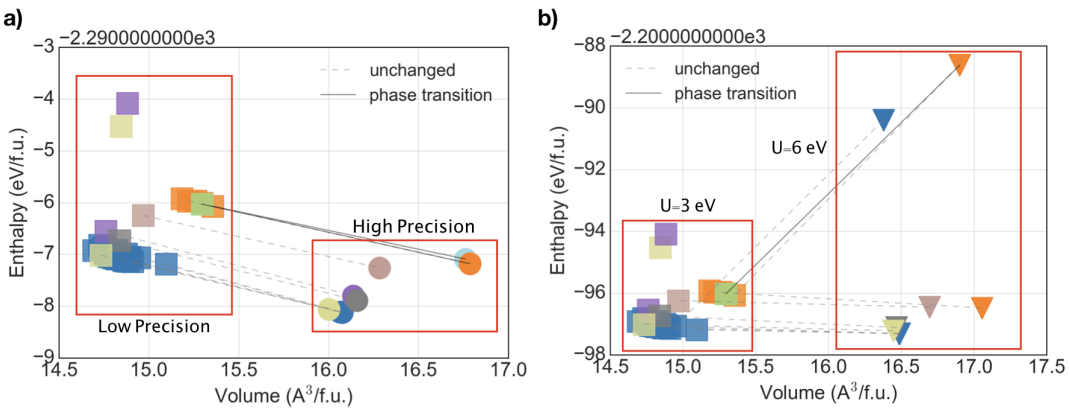


FIG. S2. AIRSS generated phases of SmH2 at 200 GPa. Squares and circles indicate phases of SmH2. Color indicates space group. Square indicate relevant DFT+U settings is "step 1" as mentioned in the main paper and circles represent "step 2". X axis is volume of the unit cell and Y axis is DFT+U calculated enthalpy. Phases in both "Low Precision and (b) "U=3eV" boxes are same group of phases and DFT+U settings are indicated are "step 1" in the method section. (a) DFT settings changed between "Low Precision" ("step 1") to "High Precision" ("step 2") but Hubbard U is kept same. (b) DFT settings changed as in (a) but Hubbard U involved in DFT+U calculation changed from 3 eV to 6 eV.

TABLE I. Lattice parameters of Sm_xH_y

	Space group	Lattice Parameters Å	Atom	Atomic fractional coordinates		
				X	Y	Z
SmH_2 (200 GPa)	$P6/mmm$	a=b=2.691931 c=2.561747 $\alpha=\beta=90°$ $\gamma=120°$	Sm(1a) H(2d)	0.000000 1/3	0.000000 2/3	0.000000 1/2
SmH_4 (200 GPa)	$I4/mmm$	a=b=2.54632297 c=5.61849941 $\alpha=\beta=\gamma=90°$	Sm(2a) H(4e) H(4d)	0.000000 0.000000 0.000000	0.000000 0.000000 1/2	0.000000 0.660104 3/4
SmH_4 (100 GPa)	$C2/m$	a=b=2.691931 c=2.561747 $\alpha=\beta=90°$ $\gamma=120°$	Sm(2a) H(4i) H(4i)	0.000000 0.098982 0.401017	0.000000 1/2 0.000000	0.000000 0.545504 0.454495
SmH_4 (140 GPa)	$Fmmm$	a=3.7920738 b=4.141084 c=5.238472 $\alpha=\beta=\gamma=90°$	Sm(4b) H(8f) H(8i)	0.000000 3/4 1/2	0.000000 3/4 1/2	1/2 3/4 0.073424
SmH_6 (140 GPa)	$Im-3m$	a=b=c=3.603054 $\alpha=\beta=\gamma=90°$	Sm(2a) H(12d)	1/2 1/2	1/2 1/4	1/2 0.000000
SmH_{10} (400 GPa)	$Fm-3m$	a=b=c=4.76101509 $\alpha=\beta=\gamma=90°$	Sm(4a) 8(c) 32(f)	1/2 1/4 0.380417	0.000000 1/4 0.380417	1/2 3/4 0.380417

II. DFT+DMFT CALIBRATION

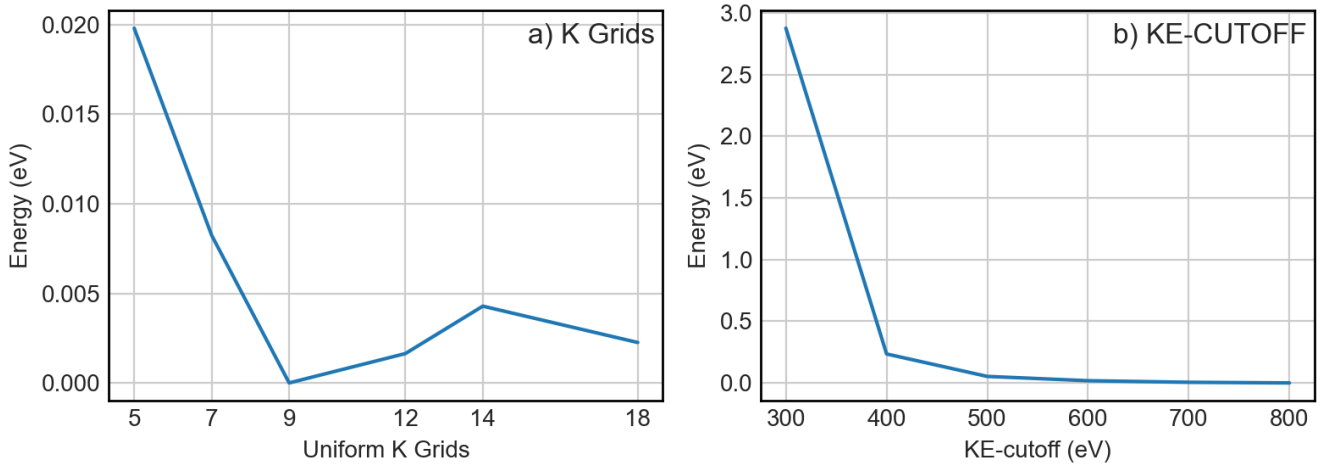


FIG. S3. DFT Convergence test: a) K-points test. KE-cutoff 400eV with XC functional PBE. b) KE cut-off test with K-points grids 14 14 14 and XC functional PBE.

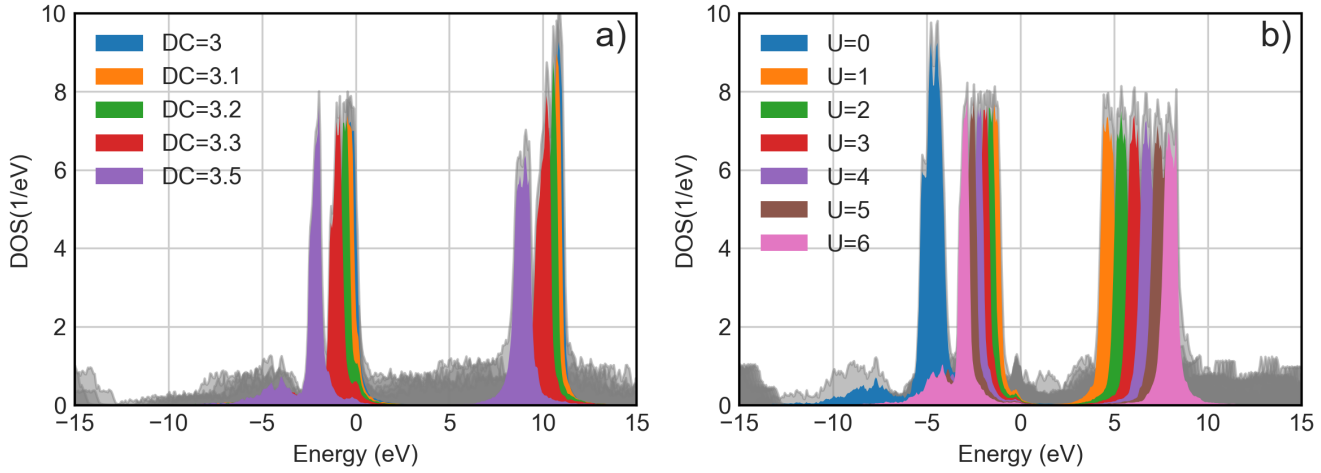


FIG. S4. (a) DC test with DFT+DMFT CSC DOS for $P6/mmm$ SmH_2: Hubbard U equal to 6eV and Hund's coupling J equal to 0.855eV (b) Hubbard U test with 1-shot DOS for $P6/mmm$ SmH_2: DC 3.5 and Hund's coupling J 0.855. Notice that Converged DC for $P6/mmm$ is around 3.1

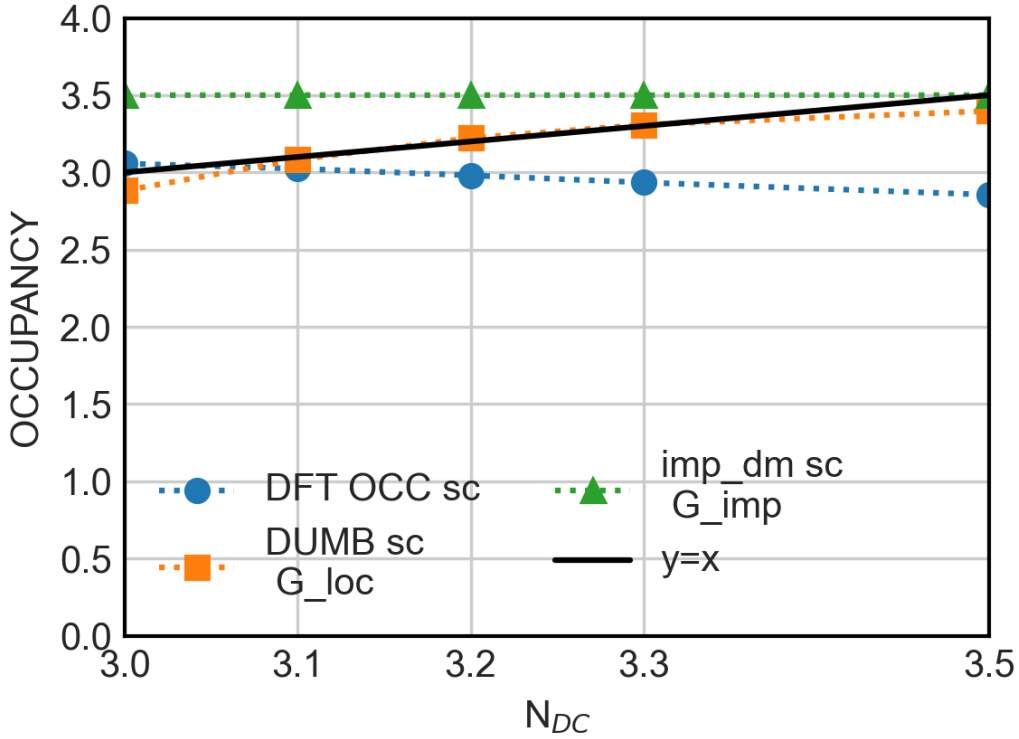


FIG. S5. DC convergence test for $P6/mmm$ with DFT+DMFT settings that, KE cutoff 600eV, kpoints used to sample the BZ is 14 14 by 9, Hubbard U 6.0 eV and Hund's coupling J 0.855 eV